Sensing of the Molecular Spin in Spin-Crossover Nanoparticles with Micromechanical Resonators

Dugay, Julien; Giménez-Marqués, Mónica; Venstra, Warner J.; Torres-Cavanillas, Ramón; Sheombarsing, Umit N.; Manca, Nicola; Coronado, Eugenio; Van Der Zant, Herre S.J.

DOI
10.1021/acs.jpcc.8b10096

Publication date
2019

Document Version
Final published version

Published in
Journal of Physical Chemistry C

Citation (APA)
Dugay, J., Giménez-Marqués, M., Venstra, W. J., Torres-Cavanillas, R., Sheombarsing, U. N., Manca, N., Coronado, E., & Van Der Zant, H. S. J. (2019). Sensing of the Molecular Spin in Spin-Crossover Nanoparticles with Micromechanical Resonators. *Journal of Physical Chemistry C*, *123*(11), 6778-6786. https://doi.org/10.1021/acs.jpcc.8b10096

THE JOURNAL OF PHYSICAL CHEMISTRY C

Article

Cite This: J. Phys. Chem. C 2019, 123, 6778−6786

pubs.acs.org/JPCC

Sensing of the Molecular Spin in Spin-Crossover Nanoparticles with Micromechanical Resonators

Julien Dugay,*[,†] Mónica Giménez-Marqués,[‡] Warner J. Venstra,[†] Ramón Torres-Cavanillas,[‡] Umit N. Sheombarsing,[†] Nicola Manca,[†,§] Eugenio Coronado,*[,‡] and Herre S. J. van der Zant[†]

[†]Kavli Institute of Nanoscience, Delft University of Technology, Lorentzweg 1, 2628 CJ Delft, The Netherlands

[‡]Instituto de Ciencia Molecular (ICMol), Universidad de Valencia, c/Catedrático José Beltrán, 2, 46980 Paterna, Spain

[§]Physics Department, University of Genoa, Via Dodecaneso 33, 16146 Genova, Italy

Supporting Information

ABSTRACT: In the past years, the use of highly sensitive silicon microelectromechanical cantilevers has been proposed as a tool to characterize the spin-crossover phenomenon by employing fast optical readout of the motion. In this work, Fe^{II}-based spin-crossover nanoparticles of the well-known $[Fe(Htrz)_2(trz)](BF_4)$ complex wrapped with thin silica shells of different sizes will be studied by means of silicon microresonators. The silica shell will enhance its chemical stability, whereas the low thickness will allow a proper mechanical coupling between the cantilever and the spin-crossover core. To maximize the sensing of the spin-crossover phenomena, different cantilever geometries and flexural modes were employed. In addition, the experimental observations were also compared with COMSOL numerical simulations, which are in close agreement with them. The probe of spin-crossover phenomena with micro- and nanoelectromechanical actuators offers the possibility of preparing smart sensing memory devices near/above room temperature.

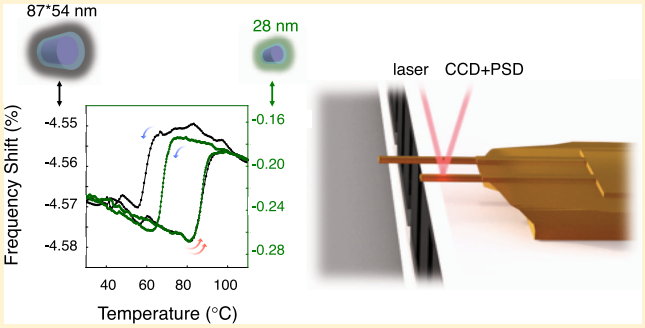

INTRODUCTION

Micro- and nanomechanical systems can be treated largely within the framework of bulk elasticity theory. This field has been under development for over half a century[1] with growing interest driven by the tremendous amount of potential daily-life applications.[2] The development of the atomic force microscope in the mid-1980s has sparked the advent of micro−nano cantilever-based platforms for physical, chemical, and biological sensing.[3−5] The operation of micro- and nanoelectromechanical sensors (MEMS/NEMS) involves measurements of static deflections, dynamical resonant frequency, or damping characteristics of the resonators. Their mechanical responses are caused by a gradient of mechanical stress that can be generated by (i) changes in temperature (in particular for cantilevers made of two layered materials with different thermal expansion coefficients),[6] (ii) molecular adsorption and interfacial chemical reactions[7] or (iii) materials showing solid-state phase transitions with an associated lattice expansion of up to 1%.[6,8,9]

The high-stress sensitivity of MEMS/NEMS for elaborating smart molecular actuators has been proposed only recently,[10−13] with one example reported in 2016 for silicon MEMS cantilevers covered with thermally evaporated spin-crossover (SCO) thin films.[14] In particular, SCO materials are interesting systems in this respect, as they show a substantial change in molecular volume and shape while adapting to environmental perturbations (e.g., up to 13%).[15] This change results from an entropy-driven switching from a low-spin state ($S = 0$, volume reduced) to a high-spin state ($S = 2$, expanded volume)[16] that can be translated into mechanical work.[17] Moreover, their physicochemical properties (electronic, optical, mechanic, and magnetic) can be adjusted and tuned to specific target applications by external stimuli such as temperature and pressure variations, light irradiation, magnetic field[18] and electric field,[19] or chemical species.[20] Furthermore, these materials enable low-cost efficient production and self-assembly techniques on various substrates.[21,22]

Two key works demonstrated the realization of micro-mechanical resonators controlled by temperature. Urdampilleta and coauthors employed an organic MEM device made of a polyethylene naphthalate substrate covered with poly-(vinylidene fluoride−trifluoroethylene), sandwiched between two thin layers of aluminum.[23] Such a device is associated with a low Young's modulus and a high aspect ratio, demonstrating large resonance frequency shifts (sometimes accompanied by hysteresis loops), dominated by the total surface stress, which is consistent with our work. Besides, Manrique-Juàrez et al. demonstrated an upward bending of the cantilever upon a low-

Received: October 16, 2018
Revised: February 24, 2019
Published: February 26, 2019

DOI: 10.1021/acs.jpcc.8b10096
J. Phys. Chem. C 2019, 123, 6778−6786

spin to high-spin transition in agreement with the change in the lattice parameters of their complex (corresponding to a compressive strain of about −1% estimated along the cantilever length).[14] Besides, they reported a decrease of approximately 66 Hz in the resonance frequency as well as a drop in the quality factor around the spin transition. In both cases, the memory effects in SCO films (with thicknesses ranging between 0.14 and 4 μm) were observed well below room temperature.

In this work, we exploit sensitive Si MEMS cantilevers to study a set of hybrid core−shell SCO nanoparticles (NPs) by employing fast optical readout of the motion of microcantilevers. We coated these microresonators with thin films of hybrid SCO@SiO_2 NPs by the drop-casting method. The NPs were made from the reference one-dimensional Fe^{II}-based SCO complex of formula $[Fe(Htrz)_2(trz)](BF_4)$, offering notably wide hysteresis in their physical properties' transitions even above room temperature.[24−26] These SCO NP cores, tunable in size, were wrapped with, particularly, thin silica (SiO_2) shells to provide enhanced chemical stability while allowing mechanical coupling with the cantilevers.[27] We investigated four different cantilever geometries and their respective three lowest resonant frequency flexural modes for SCO detection. While the cores of the SCO NPs switch from the low-spin to the high-spin state, a systematic and reversible increase in the cantilever resonance frequency was observed. Concomitantly, a drop in the quality factor and static bending of the cantilever was revealed. The experimental observations are corroborated by a finite-element analysis, which quantitatively reproduces the temperature dependence of the resonant frequencies and static deflections of the hybrid SCO@SiO_2 NPs.

METHODS

Synthesis of Hybrid $[Fe(HTrz)_2(Trz)](BF_4)$@SiO_2 NPs. For the synthesis of hybrid SCO NPs **1** and **2**, we followed a modified protocol of the reverse-micelle synthesis[27] developed by Herrera and Colacio and co-workers. Parameters such as the concentration of SCO precursors ($Fe(BF_4)_2{\cdot}6H_2O$ and 1,2,4-1*H*-triazole) and the addition of the SiO_2 precursor to the organic phase were selectively modified to respectively tune both the size of the SCO core and the thickness of the inorganic shell. In a general procedure, two microemulsions containing aqueous solutions of the precursors, $Fe(BF_4)_2{\cdot}6H_2O$ (0.5 mL, 1.25 M in the case of NPs 1 and 1.5 M in the case of NPs 2) and the ligand 1,2,4-1*H*-triazole (0.5 mL, 3.75 M for 1 and 4.5 M in 2), were prepared by mixing with an organic solution of Triton X-100 (1.8 mL, ω = 9 for 1 and 2.2 mL, ω = 5 in 2), *n*-hexanol (1.8 mL), tetraethyl orthosilicate (0.1 mL), and cyclohexane (7.5 mL). The microemulsions were mixed and left to react for 24 h in 1, whereas they were only stirred for 2 h in 2. NPs were collected after precipitation by adding acetone to destabilize the microemulsion, followed by four washing cycles with ethanol to remove the excess surfactant, and one with acetone. Finally, the powdered samples were dried at 70 °C for 2 h.

Deposition of NPs on Microcantilevers. Tipless silicon cantilevers (All-In-One, Budget Sensors) were used with four distinct geometries listed in Table S2. The cantilevers were decorated with silica (SiO_2)-coated NPs using the drop-casting method (the deposition is performed only on one side of the cantilever). This deposition technique is well suited for the present NP systems, since the SCO active cores are stabilized by a polar SiO_2 shell. To obtain sufficient coverage, we adjusted the colloidal solution concentration by the following two steps. First, 5 mg of dry SCO@SiO_2 NP powder was suspended in 2 mL of ethanol and stirred in an ultrasonic bath for 15 min. Ethanol has a low boiling point and is polar, and readily disperses the SCO@SiO_2 NPs. A concentration of 2.5 mg/mL showed good stability over time with no signs of precipitation. In the second step, the suspension was diluted 100 times in ethanol and drop-cast onto the chip using a micropipette. The excess liquid was removed with absorbing paper, and most of the remaining solvent evaporated during thermal cycling in vacuum, as is discussed in the main text.

Deposition of Ethanol on Microcantilevers. A similar device was prepared for acting as a reference for the study by drop-casting ethanol onto the chip. The excess liquid was removed with absorbing paper, and most of the remaining solvent evaporated during thermal cycling in vacuum, as is discussed in the main text.

Measurement of the Temperature-Dependent Mechanical Response. *Measurement of the Mechanical Response.* An optical lever is used to detect the static and dynamic displacements of the cantilevers. The cantilevers are placed in a small vacuum chamber to reduce viscous air friction and potential contamination of the SCO NP layer. The cantilevers are mounted on a manual positioning stage, which enables the selection of the cantilever of interest. The resonance modes are excited by supplying the alternating voltage from a network analyzer (Agilent 4395A) to a piezoactuator (Piezo Systems Inc.) placed in the vicinity of the cantilever chip. The signal from a power spectral density (PSD) was detected by the network analyzer and recorded on a computer. The measurements are conducted at a pressure of 2×10^{-6} mbar, while the excitation voltages are low enough to ensure that the cantilever vibrates in the linear regime. The static bending of the cantilever is detected by measuring the direct current (dc)-component of the PSD voltage using a multimeter (Keithley DMM199). The incident probe laser power is well below 1 mW, so as to eliminate the effects of laser heating.

Temperature Control Details. The temperature of the chip is determined by measuring the resistance of an negative temperature coefficient placed close to the chip on the Peltier element. A proportional integral derivative controller is implemented in LabView, and a custom-built power amplifier is employed to drive the Peltier element toward the temperature setpoint. To remain in the quasi-static measurement regime, all temperature sweeps are performed at 1 °C/min, and the temperature variation during a frequency response measurement is below 0.1 °C over a range of 15−135 °C. This range covers the temperatures at which the hysteretic SCO is expected.

Figure 1 describes the optical lever system. The output of a temperature-stabilized laser diode, emitting at 658 nm, enters through a polarizer and passes through a polarizing beam splitter (PBS) and a quarter wave plate. The beam is directed onto the cantilever of interest, which can be selected by adjusting the position of the vacuum chamber containing the cantilevers with a micropositioning stage, while monitoring the cantilever position using a camera. The reflection of the cantilever surface passes again through the $\lambda/4$ plate and is deflected by the PBS onto the position-sensitive device (PSD). To detect the mechanical response, the cantilevers are excited by supplying the output of a vector network analyzer (VNA) to

DOI: 10.1021/acs.jpcc.8b10096
J. Phys. Chem. C 2019, 123, 6778−6786

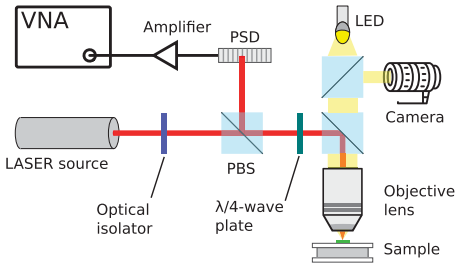

Figure 1. Schematic of the optical lever system. PBS: polarizing beam splitter; PSD: position-sensitive device; LED: light-emitting diode.

a piezoactuator placed near the sample in the vacuum chamber. The magnitude- and phase response of the cantilever to the excitation signal is detected by the network analyzer and recorded on a computer (see Methods for more experimental details).

Errors in Measurements. Besides, the error results on our data are comparable with the marker size. Indeed, the error on the frequency measurements can be evaluated, considering the spectrum sampling density of the vector network analyzer, which is selected at the measurement time and corresponds to 10 Hz. The temperature is not calibrated, so the error is evaluated considering the temperature fluctuations (noise) of the temperature sensor, which are below 50 mK. The error on the COMSOL simulations is not statistical and is given by the selected convergence criterion, well below 10^{-3}. All of these values are not visible in the reported plots and are thus not included.

RESULTS AND DISCUSSION

Before depositing the SCO NPs, the temperature dependence of the mechanical properties of the bare cantilevers was characterized. Figure 2a shows the resonance frequencies of the fundamental mode (chip A, cantilever B), obtained by fitting a harmonic oscillator to the detected frequency responses. The resonance frequency decreases in proportion with the temperature (−2 Hz/°C), which is expected from the temperature dependence of the elastic modulus of silicon in this temperature range.[8] The quality factors being almost temperature independent, see the inset, indicated that the silicon cantilevers vibrate in the intrinsic damping regime,[28] i.e., the major damping processes occur in the cantilever, whereas the medium has a negligible effect. Comparable responses were obtained for higher flexural resonance modes and for the other cantilevers on the same chip (see Figures S4 and S5). A finite-element model of the coupled thermal−mechanical problem captures the temperature dependence of the resonance frequency, as is shown by the black thin line in Figure 2a, and is also in good agreement with the other cantilever geometries (see Figures S4 and S5).

We selected NPs based on the renowned $[Fe(Htrz)_2(trz)](BF_4)$ (Htrz = 1,2,4-triazole and trz = 1,2,4-triazolate) SCO material. It has already been established that a shell of SiO_2 grown around the NP confers robustness and allows functionality.[29,30] For application in MEMS sensors, it is important that the interaction of the NPs with the cantilever is maximized. For this reason, we obtained a set of hybrid SiO_2-SCO NPs presenting different sizes surrounded by a very thin inorganic shell of only a few nanometers, enough to protect and preserve the SCO core, while allowing for sufficient interaction with native oxide of the Si cantilever (see Methods for experimental details of the synthesis). The NPs **1** and **2** in this study exhibit different sizes (prismatic shape with dimensions 87 × 54 nm^2 and cubic shape with dimension 28 nm covered with a SiO_2 shell of 1 and 0.5 nm, respectively), as confirmed by transmission electron microscopy (TEM) characterization (Figure S1). Deposition proceeded by first suspending the SCO NPs in pure ethanol and drop-casting them on top of the cantilevers (see Methods for details of NP deposition); additionally, as a reference, a device covered with pure ethanol was fabricated, following the same method. Scanning electron microscopy (SEM) inspection of, e.g., chip A, carried out after drop-casting and numerous mechanical measurements as a function of temperature, demonstrated the presence of noncoalesced SCO NPs not only on the chip but also on all cantilevers (see Figures S1b and S7).

The discussion below will focus primarily on NPs **1**. Some results on NPs **2** will be reported for comparison at the end of the section. Drop-casting a suspension of SCO NPs on a cantilever introduces frequency shifts due to the added mass of the NPs and of the solvent. To distinguish these effects from signals that are associated with the intrinsic behavior of the SCO NPs, we first examined the effect of depositing the

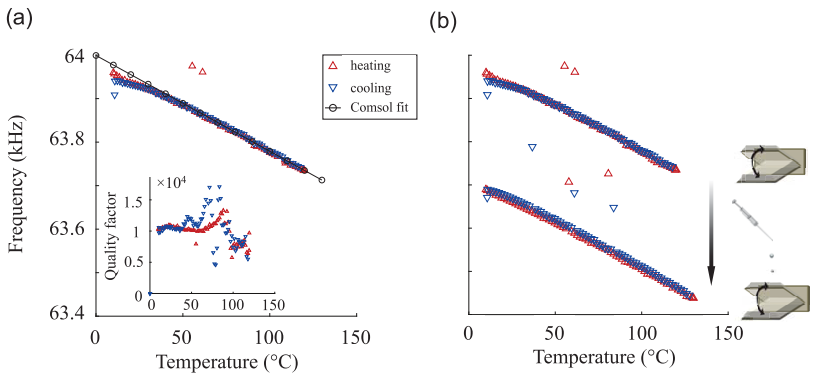

Figure 2. (a) Resonance frequency of the bare cantilever (chip A, cantilever B, fundamental mode) across the temperature range of interest. The experiment shows one cycle of controlled heating (red triangles pointing upward), followed by controlled cooling (blue triangles pointing downward). The black solid line represents a finite-element model (see the main text). Over the temperature range 15−135 °C, the resonance frequency varies by 0.5%. The associated quality factor is presented in the inset. (b) Adding the solvent (ethanol) causes the overall response shifting to a lower frequency. After preconditioning the cantilever by 15 thermal cycles, the response stabilizes at a residual frequency shift of −260 Hz.

DOI: 10.1021/acs.jpcc.8b10096
J. Phys. Chem. C 2019, 123, 6778−6786

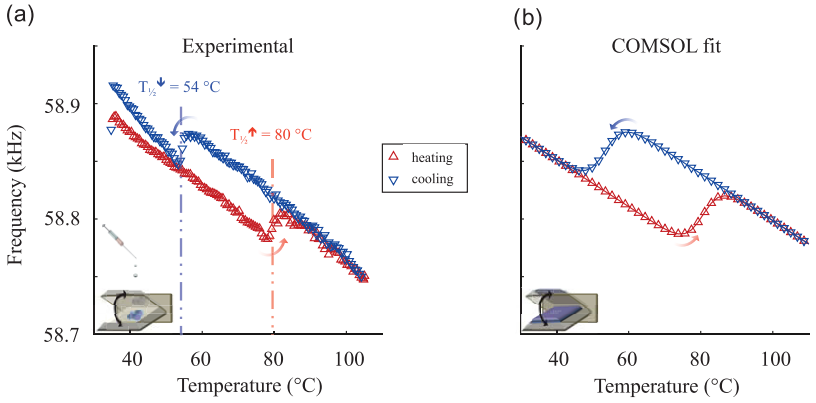

Figure 3. Comparison of experimental (a) and simulated (b) thermal hysteresis loops detected in the fundamental resonance frequency of hybrid resonators. On the left, hybrid SCO NPs (sample **1**, see the Supporting Information) are covering the cantilever type (the same sample as in Figure 2). The data presented correspond to the seventh thermal cycle reproducibly observed after preconditioning (consisting of 15 thermal cycles); the change in frequency corresponds to the mass addition of 3.44 ng. Simulations were carried out by approximating this mass to a homogeneously distributed thin layer covering the cantilever, where the latter is endowed with the same spin-dependent physical properties as the SCO NPs **1** (see Table S4 in the Supporting Information). A good agreement between experimental and numerical results is obtained when the thickness of the thin layer is set to 650 nm.

solvent. A significant drop in the resonance frequency was observed after the deposition, which diminished as the solvent evaporated while cycling the temperature and then stabilized at −260 Hz after 15 temperature cycles. Figure 2b shows the stabilized (after 15 cycles) temperature dependence of the resonance frequency (lower curve) in comparison to the bare cantilever (upper curve). The downward shift was attributed to remaining adsorbed solvent molecules, whose total mass Δm can be calculated from the frequency shift Δf as $\Delta m = -2\Delta f/f_0 \times m_0$, where m_0 = 23.1 ng is the mass of the cantilever and f_0 = 63.93 kHz is the resonance frequency of the bare cantilever.[31] The mass of the remaining adsorbed solvent molecules was estimated to be about 0.19 ng.

Figure 3 displays the fundamental resonance frequency recorded after nanoparticle deposition and after thermal preconditioning (six times reproduced thermal hysteresis loops; the same sample as the one used in Figure 2).

Considering the resonant frequency shift observed after depositing the NPs by drop-casting, we evaluate that the mass of the added NPs is equal to 3.44 ng corresponding to a frequency shift of 4.8 kHz. This frequency shift corresponds to the subtraction of the resonant frequency before and after drop-casting of the colloidal solution of SCO NPs and after stabilization under similar conditions and using the same cantilever (see Figures 1b and 2a). This mass corresponds to a NP volume of about 1.9×10^{-6} mm^3 in the low-spin state. Note that the slight shift observed after solvent drop-casting was beforehand subtracted from the total resonance frequency shift. Assuming that the top face and both undercut sides of the cantilever are uniformly covered with the NPs and that their lengths are aligned within the monolayers (MLs), we estimated that the thickness of the resulting thin film falls in the range of 330−360 nm (corresponding to about six monolayers (MLs); see calculation details in the Supporting Information). This estimation seems plausible in view of the SEM observations reporting the presence of NP islands sometimes thicker than ca. 6 MLs (see Figures S1b and S7 in the Supporting Information).

In Figure 3a, a slight decrease in the resonance frequency with increasing temperature of about 0.34% over 70 °C (i.e., of about −2.5 Hz/°C) was observed. This value is very close to the linear contribution revealed earlier from the reference cantilever (of about −2 Hz/°C, see Figure 2). More remarkable than the background contribution was the appearance of a well-pronounced and reproducible hysteresis loop in the temperature dependence of the resonance frequency. The transition temperature onset above room temperature is in agreement with the magnetic measurements obtained on powder samples (see Figure S3 and Table S1 in the Supporting Information) and transport measurements using graphene nanogaps.[32] We emphasize that control experiments revealed that hysteresis loops in the resonance frequency were neither observed for the same cantilever as-received nor after deposition of drops of pure ethanol (see Figure 2). We thus rationalize that the bistable mechanical response accompanied by wide hysteresis loops corresponds to the spin-state-dependent physical properties of the investigated hybrid SCO@SiO_2 NPs.

Another important observation in Figure 3 is the abrupt increase of the resonance frequency when the SCO NPs undergo the LS → HS transition (and vice versa while decreasing the temperature). This corresponds to a frequency change of about 30 Hz for cantilever B of chip A (or 4.3×10^{-2}%). This behavior seems, at a first glance, to be in contradiction with a recently published work reporting a slight opposite downshift of −0.5 Hz (or 1.18×10^{-2}%), detected using thicker microcantilevers.[14] We attribute the observed upshift upon the low-spin to high-spin thermal transition to the predominant role of the surface stress when thin structures are probed. In particular, the substantial volume increase of the SCO@SiO_2 NPs in the high-spin state leads to a larger curvature and therefore effective rigidity of the cantilever. This, in turn, causes the increase observed in the resonant frequency. As only one simplified analytical model has been developed to account for this phenomenon,[14] we calculated the resonance frequencies of the hybrid resonators with a finite-element-based numerical model.

Indeed, the temperature dependence of the resonance frequencies of the composite SCO@SiO_2 NPs/cantilever was calculated numerically using the structural mechanics module of COMSOL Multiphysics 5.2. The cantilever geometry was parametrized in MATLAB and transferred via LiveLink

DOI: 10.1021/acs.jpcc.8b10096
J. Phys. Chem. C 2019, 123, 6778−6786

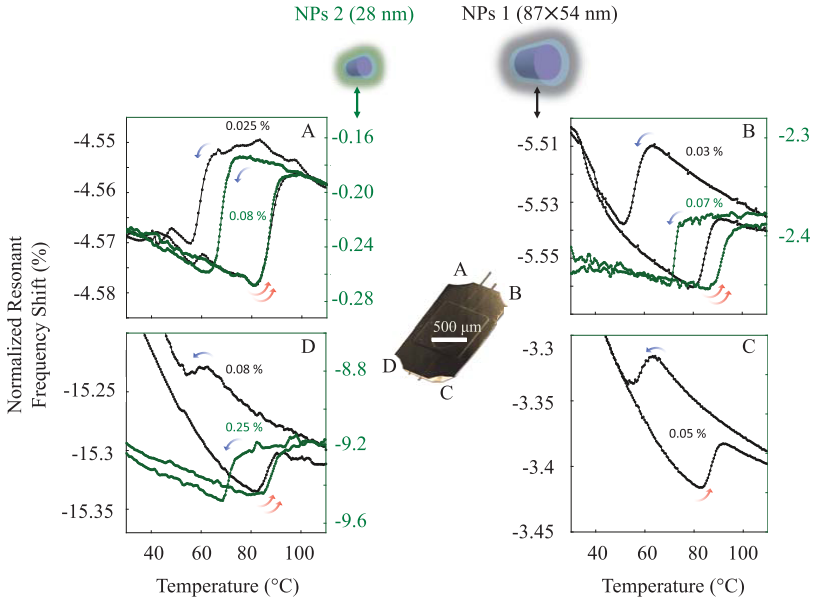

Figure 4. Normalized resonant frequency shift of SCO@SiO_2/Si microcantilevers as a function of temperature for the four cantilever geometries (chips B and C). The shift and normalization are with respect to the first flexural resonant frequency of the bare cantilevers. These data were acquired after thermal preconditioning (of about 15 thermal cycles) and reproduced multiple times. The wide thermal hysteresis loops in the mechanical responses near room temperature correlate with the SCO@SiO_2/Si NP morphologies. This behavior was consistently observed for the first, second, and fifth flexural vibrational eigenmode.

MATLAB to COMSOL. Both the static bending and the dynamic response (multiple flexural modes) were calculated for the four cantilevers, coated with SCO NP films having variable thickness. The three-dimensional (3D) models closely resemble the genuine cantilever geometry. For convenience, the "picket"-shaped end of the cantilever was simplified to a rectangular shape. The material properties used for the model are listed in the Table S2.

This numerical model allows us to simulate genuine stress softening, geometric changes, and temperature dependence of a MEMS device covered with a SCO thin film of tunable thickness, which were determined by accurate analysis using numerical simulations (see Methods for details). In the calculations, we assume a homogeneously distributed thin NP layer with a thickness corresponding to the one estimated from the resonant peak shifts. The physical properties used for the SCO@SiO_2 NPs are summarized in Table S4. The thin-film thickness is varied from about one hybrid NP monolayer (ML) up to about 5 μm. The resulting numerical simulations substantiate the experimental upshifts of the resonance frequency observed upon the LS → HS transition, as displayed in Figure 3b (see the Figure S3). The anticlockwise loop direction observed experimentally is consistent with our numerical results, which also predict an anticlockwise loop direction for SCO films with thicknesses below 3.6 and 1.8 μm, respectively, for samples 1 and 2. For thicker films, an inversion of the hysteresis loop direction from anticlockwise to clockwise is expected. The simulated resonance frequency shift and the relative change in resonance frequency as a function of temperature are in very good agreement with experimental results if the NP layer thickness is set to 650 nm. This value is within a factor of 2 compared to the one experimentally estimated from the change in frequency.

Numerous parameters can affect the cantilever resonance frequencies, such as (i) fabrication-related factors (geometry of cantilevers and thickness nonuniformity), (ii) the surface state at the interface between the cantilever and the covering material, (iii) the change in mechanical properties of the covering material (Young's modulus, mass density, and thermal dilatation), and (iv) extrinsic factors (adsorbed masses, ambient pressure, and temperature).[31] When fabricated and measured under similar conditions, it is expected that the changes in surface stresses govern the resonance frequency shift for thin structures when b (width)/h (thickness) $\gg$ 1, whereas a change in geometry due to elastic deformation or a volume change of a covering layer will prevail for thicker devices.[33]

To shed more light on the mechanism behind the frequency changes and hysteresis, similar experiments were performed with smaller NPs (sample 2) and with cantilevers with different b/h ratios. In Figure 4, we present the lowest flexural resonant frequency shifts as a function of temperature for both NPs, **1** and **2**. The temperature-dependent elastic modulus of the bare cantilevers is eliminated by subtracting the resonant frequency at a given cantilever geometry before NP deposition from that observed after NP deposition and normalized to the bare cantilever values, in each case at the same temperature. Remarkably, for both NP morphologies, clear thermal hysteresis loops are observed for each of the four cantilever geometries (see Table S2 for cantilever dimensions). Similar anticlockwise and wide thermal hysteresis loops are consistently seen, not only for the lowest flexural eigenmode but also for the second and fifth ones (for the longest cantilevers, see for instance Figure S11). Note that the normalized shift in the resonance frequency upon spin transitions follows the cantilever resonance frequency, which increases when the cantilever length is reduced (from 0.025 to 0.08 and 0.08 to 0.25% for **1** and **2**, respectively, as displayed in Figure 4).

The frequency shift arises from the mechanical expansion of SCO NPs upon spin transition and the consequent mechanical stress applied to the cantilever surface. The frequency shift is a result of the dynamical interaction between localized stress and

DOI: 10.1021/acs.jpcc.8b10096
J. Phys. Chem. C 2019, 123, 6778−6786

structural deformation, i.e., it matters whether the SCO NPs are located in a node of the eigenfunction of a particular mode or not. Changing the modes and length makes the nodes to be located in different positions and thus results in different frequency shifts. When comparing the numerical and experimental results, we conclude that smaller cantilevers exhibit the best sensitivity in terms of detection in the change of surface stress and accompanying shift in the mechanical eigenfrequencies upon the SCO transition, which is in good agreement with our experimental observations (see Figure S13). Moreover, better sensitivity is expected for higher flexural modes, which is also observable in our measurements (see Figures S14 and S12, respectively, for numerical simulation and experimental results). The amount of frequency increase is determined by the balance between the total rigidity of the structure and the accumulated stress.[33] The structural rigidity is determined by the geometry of the cantilevers; a higher sensitivity is expected for cantilevers with a larger surface/volume ratio. The accumulated stress is enhanced for the highest vibrational modes and modified by the change in volume of the NPs upon the SCO transition.

To investigate the SCO temperatures in more detail, we collected the detected transition temperatures—which turned out to be independent of the cantilever geometry and vibration mode—and plotted them in a histogram. Figure S15 compiles the experimental set of 152 measured SCO transition temperatures in cooling ($T^{LS\leftarrow HS}$, blue) and heating ($T^{LS\rightarrow HS}$, red) modes. The transition temperatures were extracted for NPs **1** (43 thermal cycles, black curve) and **2** (33 thermal cycles, green curve). Statistically, a clear NP size effect on the transition temperatures is demonstrated, where the expectation value of $T^{LS\rightarrow HS}$ is 57 °C for **1**, whereas for **2**, the transition occurs at T = 72 °C; for $T^{LS\leftarrow HS}$, the expectation values are 85 and 90 °C for **1** and **2**, respectively.

These transition temperatures can be compared with those of superconducting quantum interference device (SQUID) measurements, as both approaches employ quasi-static measurements (see Methods). Interestingly, slight shifts toward lower temperatures and narrower width loops are observed when compared with SQUID measurements. Moreover, ($T^{LS\leftarrow HS}$ is size independent and $T^{HS\rightarrow LS}$ is size dependent), whereas the opposite behavior is observed for transition temperatures extracted from SQUID measurements. One cannot exclude that the differences in sample environmental pressure of the two types of experiments cause the slight mismatch in transition temperatures: SQUID magnetometry is performed under a few mbar partial He pressure, whereas the MEMS measurements presented in this paper are performed under a high vacuum of about 2×10^{-6} mbar. It is known that a decrease in the pressure reduces the transition temperatures of SCO compounds.[34,35] However, the downward shift is expected to be negligible for this pressure range and should occur in a symmetric way,[36] which is not the case. We thus speculate that the difference in SCO transition temperatures, when comparing powdered samples (SQUID measurements) and small assemblies of hybrid SCO NPs, may be due to a difference in interparticle elastic interactions (3D vs 2D respectively) and/or to the mechanical coupling with the supporting silicon cantilever. Both contributions could modify the elastic surface stress, resulting in a volume misfit change between the SCO core and the SiO_2 shell of the NPs. Indeed, the interplay between lattice vibrational and mechanical features of the core−shell NP is the prominent mechanism for memory effect features.[37,38] On the other hand, one cannot rule out that acoustic phonons emitted from the environment (not necessarily similar in a SQUID or in a MEMS setup) are more prone to efficiently couple to the phononic density of states spectrum of the core−shell NPs rather than the optical ones.[39] However, a comprehensive theoretical study encompassing the elastic interactions between core−shell NPs in direct contact with a supporting substrate is not yet available in the literature. Such an effect has thus to be more thoroughly investigated both theoretically and experimentally.

A change in the surface stress accumulation not only affects the resonance frequency but also the static curvature of the cantilever. For this reason, we also detected the static deflection of the cantilevers by measuring the dc-component of the signal from the position-sensitive device (see Figure S10b in the Supporting Information).[40] A rather large background slope is introduced upon heating the setup, which causes a rotation of the chip due to thermal expansion mismatch. On top, a clear hysteresis is observed in the cantilever curvature, which occurs at the same temperatures as in the dynamic measurements. The spin-state dependence of the signal cannot arise from the well-established spin-state dependence of the optical absorption of the triazole-based SCO compound,[41] as these compounds absorb a little bit more (and thus reflect less) at the laser wavelength upon LS → HS crossover, whereas the opposite behavior is observed (e.g., a more reflected signal). As a control experiment, a bare cantilever was measured under the same conditions, displaying solely the exponential decrease upon increasing the temperature (see Figure S10a in the Supporting Information).

It is also of interest to investigate the damping characteristics of the cantilevers as a function of temperature. The damping figure of merit is embodied by the quality factor of the resonance, which represents the ratio between the total energy in the resonance mode and the energy that is dissipated per cycle. Remarkably, as is shown in Figure S8b, the Q-factor drops upon the LS → HS transition when increasing the temperature, whereas the cantilever vibrates at a higher resonance frequency. In addition, for the smallest SCO NPs **2**, we observe distinct minima in the Q-factor near the onset of the spin transition (see Figure S9b). Furthermore, for both SCO NP sizes and for all background resonance modes considered, we detect a systematic increase in the Q-factor with increasing temperature. In contrast, a linear drop usually occurs for silicon beams as the temperature is raised due to thermoelastic damping at constant pressure. As far as the drop in the Q-factor on going from the LS to the HS state is concerned, this behavior is not related to the SCO-induced internal stress (where Q would increase with the frequency) but suggests a significant increase in the damping force when the cores of the NPs are in the HS state. At this point, we can only speculate that this increase could emanate from the increased contact area (caused by the larger volume in the HS state) between the SCO@SiO_2 NPs and the cantilever, thereby enhancing the friction at the NP−cantilever interface.

While the MEMS devices here were introduced as a characterization tool, we note that the large volumetric changes of SCO materials present a significant potential for their use as actuator materials in MEMS and NEMS devices.[42] Compared to the piezoelectric actuators that are widely deployed in MEMS devices, the strain introduced by the SCO is higher (by 2−3 orders of magnitude), while the presence of hysteretic properties above room temperature enables new

DOI: 10.1021/acs.jpcc.8b10096
J. Phys. Chem. C 2019, 123, 6778−6786

actuator-and-hold schemes. These properties could be harnessed, e.g., by incorporating metallic heaters in the hybrid MEMS device.[43]

During the preparation of this manuscript we became aware of two related works in which thermo-active MEMS devices were actuated at their resonance frequency by a voltage or magnetic field, while the mechanical vibration detection was performed by piezoresistors.[23,44] The first one employed an organic MEM device made of a polyethylene naphthalate substrate covered with poly(vinylidene fluoride−trifluoroethylene), sandwiched between two thin layers of aluminum. Such a device is associated with a low Young's modulus and a high aspect ratio, demonstrating large resonance frequency shifts (sometimes accompanied by hysteresis loops), dominated by the total surface stress, which is consistent with our work.[45] Second, in a very similar manner to what we did, Manrique-Juárez et al. demonstrated an upward bending of the cantilever upon the LS → HS transition, in agreement with the change in the lattice parameters of their complex (corresponding to a compressive strain of about −1% estimated along the cantilever length). Besides, they reported a decrease of approximately 66 Hz in the resonance frequency as well as a drop in the quality factor around the spin transition.[44] In both cases, the memory effects in SCO films (with thicknesses ranging between 0.14 and 4 μm) were observed well below room temperature.

CONCLUSIONS

In this work, we used microcantilevers to detect the thermally induced cooperative spin-state switching of hybrid SCO NPs above room temperature. We employed fast optical readout of the motion of tipless silicon atomic force microscopy cantilevers with various geometries ranging from 500 to 100 ± 10 μm in length, 50 to 30 ± 5 μm in width, and 2.7 ± 1 μm in thickness.[46,47] These small resonators were decorated by drop-casting robust core−shell SCO@SiO_2 NP systems with two different morphologies (87 × 54 and 87 × 28 nm^2). When the cores of these hybrid SCO NPs switched from the low-spin to the high-spin state, a systematic and reversible increase in the cantilever resonance frequency was observed, consistently for various cantilever geometries and resonance modes. We ascribed these hysteretic behaviors to variations of the surface stress (through the molecular volume change). Concomitantly with the abrupt resonant frequency upshift in the high-spin state, a drop occurred in the quality factor and the reflected laser power. The former behavior was related to the enhanced internal friction, most likely due to the increased contact areas of the NP/cantilever interfaces upon the LS → HS state transition. The latter behavior was rationalized through the cantilever bending, as expected from the strong lattice expansion of the SCO NP upon the LS → HS state transition.

We substantiated the experimental observations with numerical simulations, providing a useful guideline for taking into account thermal effects, interfacial aspects, realistic cantilever geometry, and SCO NP parameters. Associating MEMS/NEMS and cooperative SCO materials could thus bring a new fundamental understanding regarding the genuine role of structural/mechanical properties of SCO (nano)-materials and open up new ways for smart sensing micro−nano devices retaining memory while operating at room temperature. Remarkably, this technique holds high sensitivity already at the state-of-the-art for investigation of memory effects at the nanoscale comparable to the detection limit of a micro-magnetometer prototype reported recently as small as 2×10^{-6} mm^3 (in terms of particle volume).

ASSOCIATED CONTENT

Supporting Information

The Supporting Information is available free of charge on the ACS Publications website at DOI: 10.1021/acs.jpcc.8b10096.

Schematic of the optical lever system, TEM images of SCO NPs **1** and **2**, Table S1, thermal variation of the magnetic susceptibility of **1** and **2**, Tables S2 and S3, details of COMSOL simulations, Table S4, detailed analytical calculations and estimations, SEM image, additional experimental data and numerical simulations (PDF)

AUTHOR INFORMATION

Corresponding Authors

*E-mail: julien.dugay@gmail.com (J.D.).
*E-mail: eugenio.coronado@uv.es (E.C.).

ORCID

Julien Dugay: 0000-0002-4384-1315
Mónica Giménez-Marqués: 0000-0002-4931-5711
Nicola Manca: 0000-0002-7768-2500

Notes

The authors declare no competing financial interest.

ACKNOWLEDGMENTS

M.G.-M. thanks MINECO for a post-doctoral Juan de la Cierva Incorporacion grant. We acknowledge funding from the EU (Advanced ERC grants Mols@Mols, COST Action MOLSPIN CA15128, ERC Advance Grant Mol-2D ref 788222, and RIA action COSMICS ref 766726). Financial support from the Spanish MINECO (Structures of Excellence María de Maeztu MDM-2015-0538, MAT2017-89993-R, and SMARTMOL project) is also acknowledged. We thank Giordano Mattoni for experimental help. We also thank Koen van Walstijn and Oscar Enzing for the development of the temperature cycling system. Also, R.T.-C. thanks the Spanish MINECO F.P.I. fellowship.

REFERENCES

(1) Newell, W. E. Miniaturization of Tuning Forks. *Science* **1968**, *161*, 1320−1326.
(2) Craighead, H. G. Nanoelectromechanical Systems. *Science* **2000**, *290*, 1532−1535.
(3) Binnig, G.; Quate, C. F.; Gerber, C. Atomic Force Microscope. *Phys. Rev. Lett.* **1986**, *56*, 930−933.
(4) Fritz, J.; Baller, M. K.; Lang, H. P.; Rothuizen, H.; Vettiger, P.; Meyer, E.; Güntherodt, H.-J.; Gerber, C.; Gimzewski, J. K. Translating Biomolecular Recognition into Nanomechanics. *Science* **2000**, *288*, 316−318.
(5) Lavrik, N. V.; Sepaniak, M. J.; Datskos, P. G. Cantilever transducers as a platform for chemical and biological sensors. *Rev. Sci. Instrum.* **2004**, *75*, 2229−2253.
(6) Singamaneni, S.; LeMieux, M. C.; Lang, H. P.; Gerber, C.; Lam, Y.; Zauscher, S.; Datskos, P. G.; Lavrik, N. V.; Jiang, H.; Naik, R. R.; Bunning, T. J.; Tsukruk, V. V. Bimaterial Microcantilevers as a Hybrid Sensing Platform. *Adv. Mater.* **2008**, *20*, 653−680.
(7) Berger, R.; Delamarche, E.; Lang, H. P.; Gerber, C.; Gimzewski, J. K.; Meyer, E.; Güntherodt, H.-J. Surface Stress in the Self-Assembly of Alkanethiols on Gold. *Science* **1997**, *276*, 2021−2024.
(8) Rúa, A.; Cabrera, R.; Coy, H.; Merced, E.; Sepúlveda, N.; Fernández, F. E. Phase transition behavior in microcantilevers coated

DOI: 10.1021/acs.jpcc.8b10096
J. Phys. Chem. C 2019, 123, 6778−6786

with M1-phase VO2 and M2-phase VO2:Cr thin films. *J. Appl. Phys.* **2012**, *111*, No. 104502.
(9) Manca, N.; Pellegrino, L.; Kanki, T.; Yamasaki, S.; Tanaka, H.; Siri, A. S.; Marré, D. Programmable Mechanical Resonances in MEMS by Localized Joule Heating of Phase Change Materials. *Adv. Mater.* **2013**, *25*, 6430−6435.
(10) Gural'skiy, I. A.; Quintero, C. M.; Costa, J. S.; Demont, P.; Molnár, G.; Salmon, L.; Shepherd, H. J.; Bousseksou, A. Spin crossover composite materials for electrothermomechanical actuators. *J. Mater. Chem. C* **2014**, *2*, 2949−2955.
(11) Molnár, G.; Salmon, L.; Nicolazzi, W.; Terki, F.; Bousseksou, A. Emerging properties and applications of spin crossover nanomaterials. *J. Mater. Chem. C* **2014**, *2*, 1360−1366.
(12) Manrique-Juárez, M. D.; Mathieu, F.; Laborde, A.; Rat, S.; Shalabaeva, V.; Demont, P.; Thomas, O.; Salmon, L.; Leichle, T.; Nicu, L.; Molnár, G.; Bousseksou, A. Micromachining-Compatible, Facile Fabrication of Polymer Nanocomposite Spin Crossover Actuators. *Adv. Funct. Mater.* **2018**, *28*, No. 1801970.
(13) Mikolasek, M.; et al. Complete Set of Elastic Moduli of a Spin-Crossover Solid: Spin-State Dependence and Mechanical Actuation. *J. Am. Chem. Soc.* **2018**, *140*, 8970−8979.
(14) Manrique-Juarez, M. D.; Rat, S.; Mathieu, F.; Saya, D.; Séguy, I.; Leïchlé, T.; Nicu, L.; Salmon, L.; Molnár, G.; Bousseksou, A. Microelectromechanical systems integrating molecular spin crossover actuators. *Appl. Phys. Lett.* **2016**, *109*, No. 061903.
(15) Cobo, S.; Ostrovskii, D.; Bonhommeau, S.; Vendier, L.; Molnár, G.; Salmon, L.; Tanaka, K.; Bousseksou, A. Single-Laser-Shot-Induced Complete Bidirectional Spin Transition at Room Temperature in Single Crystals of (FeII(pyrazine)(Pt(CN)$_4$. *J. Am. Chem. Soc.* **2008**, *130*, 9019−9024.
(16) Gütlich, P.; Goodwin, H. A. *Spin Crossover in Transition Metal Compounds I*; Springer Verlag, 2004; Vol. *1*.
(17) Manrique-Juárez, M. D.; Rat, S.; Salmon, L.; Molnár, G.; Quintero, C. M.; Nicu, L.; Shepherd, H. J.; Bousseksou, A. Switchable molecule-based materials for micro- and nanoscale actuating applications: Achievements and prospects. *Coord. Chem. Rev.* **2016**, *308*, 395−408.
(18) Bousseksou, A.; Molnár, G.; Salmon, L.; Nicolazzi, W. Molecular spin crossover phenomenon: recent achievements and prospects. *Chem. Soc. Rev.* **2011**, *40*, 3313−3335.
(19) Prins, F.; Barreiro, A.; Ruitenberg, J. W.; Seldenthuis, J. S.; Aliaga-Alcalde, N.; Vandersypen, L. M. K.; van der Zant, H. S. J. Room-Temperature Gating of Molecular Junctions Using Few-Layer Graphene Nanogap Electrodes. *Nano Lett.* **2011**, *11*, 4607−4611.
(20) Coronado, E.; Giménez-Marqués, M.; Mínguez Espallargas, G.; Rey, F.; Vitórica-Yrezábal, I. J. Spin-Crossover Modification through Selective CO_2 Sorption. *J. Am. Chem. Soc.* **2013**, *135*, 15986−15989.
(21) Cavallini, M. Status and perspectives in thin films and patterning of spin crossover compounds. *Phys. Chem. Chem. Phys.* **2012**, *14*, 11867−11876.
(22) Dugay, J.; Giménez-Marqués, M.; Kozlova, T.; Zandbergen, H. W.; Coronado, E.; van der Zant, H. S. J. Spin Switching in Electronic Devices Based on 2D Assemblies of Spin-Crossover Nanoparticles. *Adv. Mater.* **2015**, *27*, 1288−1293.
(23) Urdampilleta, M.; Ayela, C.; Ducrot, P.-H.; Rosario-Amorin, D.; Mondal, A.; Rouzières, M.; Dechambenoit, P.; Mathonière, C.; Mathieu, F.; Dufour, I.; Clérac, R. Molecule-based microelectromechanical sensors. *Sci. Rep.* **2018**, *8*, No. 8016.
(24) Coronado, E.; Galán-Mascarós, J. R.; Monrabal-Capilla, M.; García-Martínez, J.; Pardo-Ibáñez, P. Bistable Spin-Crossover Nanoparticles Showing Magnetic Thermal Hysteresis near Room Temperature. *Adv. Mater.* **2007**, *19*, 1359−1361.
(25) Galán-Mascarós, J. R.; Coronado, E.; Forment-Aliaga, A.; Monrabal-Capilla, M.; Pinilla-Cienfuegos, E.; Ceolin, M. Tuning Size and Thermal Hysteresis in Bistable Spin Crossover Nanoparticles. *Inorg. Chem.* **2010**, *49*, 5706−5714.
(26) Giménez-Marqués, M.; García-Sanz de Larrea, M. L.; Coronado, E. Unravelling the chemical design of spin-crossover nanoparticles based on iron(ii)-triazole coordination polymers: towards a control of the spin transition. *J. Mater. Chem. C* **2015**, *3*, 7946−7953.
(27) Torres-Cavanillas, L. R.; Lima, L.; Tichelaar, F. D.; Zandbergen, H.; Giménez-Marqués, M.; Coronado, E. Limiting the size of hybrid Fe-triazole@SiO_2 spin-crossover nanoparticles, submitted for publication, 2018.
(28) Blom, F. R.; Bouwstra, S.; Elwenspoek, M.; Fluitman, J. H. J. Dependence of the quality factor of micromachined silicon beam resonators on pressure and geometry. *J. Vac. Sci. Technol., B: Microelectron. Nanometer Struct.–Process., Meas., Phenom.* **1992**, *10*, 19−26.
(29) Titos-Padilla, S.; Herrera, J. M.; Chen, X.-W.; Delgado, J. J.; Colacio, E. Bifunctional Hybrid SiO_2 Nanoparticles Showing Synergy between Core Spin Crossover and Shell Luminescence Properties. *Angew. Chem.* **2011**, *123*, 3348−3351.
(30) Raza, Y.; Volatron, F.; Moldovan, S.; Ersen, O.; Huc, V.; Martini, C.; Brisset, F.; Gloter, A.; Stéphan, O.; Bousseksou, A.; Catala, L.; Mallah, T. Matrix-dependent cooperativity in spin crossover Fe(pyrazine)Pt(CN)$_4$ nanoparticles. *Chem. Commun.* **2011**, *47*, 11501−11503.
(31) Mahmoud, M. A. Validity and Accuracy of Resonance Shift Prediction Formulas for Microcantilevers: A Review and Comparative Study. *Crit. Rev. Solid State Mater. Sci.* **2016**, *41*, 386−429.
(32) Holovchenko, A.; Dugay, J.; Giménez-Marqués, M.; Torres-Cavanillas, R.; Coronado, E.; van der Zant, H. S. J. Near Room-Temperature Memory Devices Based on Hybrid Spin-Crossover@SiO_2 Nanoparticles Coupled to Single-Layer Graphene Nanoelectrodes. *Adv. Mater.* **2016**, *28*, 7228−7233.
(33) Karabalin, R. B.; Villanueva, L. G.; Matheny, M. H.; Sader, J. E.; Roukes, M. L. Stress-Induced Variations in the Stiffness of Micro- and Nanocantilever Beams. *Phys. Rev. Lett.* **2012**, *108*, No. 236101.
(34) Tanasa, R.; Stancu, A.; Létard, J.-F.; Codjovi, E.; Linares, J.; Varret, F. Piezo- and thermo-switch investigation of the spin-crossover compound [Fe(PM-BiA)$_2$(NCS)$_2$]. *Chem. Phys. Lett.* **2007**, *443*, 435−438.
(35) Linares, J.; Codjovi, E.; Garcia, Y. Pressure and Temperature Spin Crossover Sensors with Optical Detection. *Sensors* **2012**, *12*, 4479−4492.
(36) Diaconu, A.; Lupu, S.-L.; Rusu, I.; Risca, I.-M.; Salmon, L.; Molnár, G.; Bousseksou, A.; Demont, P.; Rotaru, A. Piezoresistive Effect in the [Fe(Htrz)$_2$(trz)](BF$_4$) Spin Crossover Complex. *J. Phys. Chem. Lett.* **2017**, 3147.
(37) Slimani, A.; Khemakhem, H.; Boukheddaden, K. Structural synergy in a core-shell spin crossover nanoparticle investigated by an electroelastic model. *Phys. Rev. B: Condens. Matter Mater. Phys.* **2017**, *95*, No. 174104.
(38) Félix, G.; Mikolasek, M.; Molnár, G.; Nicolazzi, W.; Bousseksou, A. Control of the phase stability in spin crossover core-shell nanoparticles through elastic interface energy. *Eur. J. Inorg. Chem.* **2017**, 435−442.
(39) Mikolasek, M.; Félix, G.; Peng, H.; Rat, S.; Terki, F.; Chumakov, A. I.; Salmon, L.; Molnár, G.; Nicolazzi, W.; Bousseksou, A. Finite-size effects on the lattice dynamics in spin crossover nanomaterials. I. Nuclear inelastic scattering investigation. *Phys. Rev. B: Condens. Matter Mater. Phys.* **2017**, *96*, No. 035426.
(40) Venstra, W. J.; Capener, M. J.; Elliott, S. R. Nanomechanical gas sensing with nonlinear resonant cantilevers. *Nanotechnology* **2014**, *25*, No. 425501.
(41) Lefter, C.; Tan, R.; Dugay, J.; Tricard, S.; Molnár, G.; Salmon, L.; Carrey, J.; Rotaru, A.; Bousseksou, A. Light induced modulation of charge transport phenomena across the bistability region in [Fe(Htrz)$_2$(trz)](BF$_4$) spin crossover micro-rods. *Phys. Chem. Chem. Phys.* **2015**, *17*, 5151−5154.
(42) Shepherd, H. J.; Gural'skiy, I. A.; Quintero, C. M.; Tricard, S.; Salmon, L.; Molnár, G.; Bousseksou, A. Molecular actuators driven by cooperative spin-state switching. *Nat. Commun.* **2013**, *4*, No. 2607.
(43) Privorotskaya, N. L.; King, W. P. Silicon microcantilever hotplates with high temperature uniformity. *Sens. Actuators, A* **2009**, *152*, 160−167.

DOI: 10.1021/acs.jpcc.8b10096
J. Phys. Chem. C 2019, 123, 6778−6786

(44) Manrique-Juarez, M. D.; Mathieu, F.; Shalabaeva, V.; Cacheux, J.; Rat, S.; Nicu, L.; Leïchlé, T.; Salmon, L.; Molnár, G.; Bousseksou, A. A Bistable Microelectromechanical System Actuated by Spin-Crossover Molecules. *Angew. Chem.* **2017**, *129*, 8186−8190.
(45) Urdampilleta, M.; Ducrot, P.-H.; Rosario-Amorin, D.; Mondal, A.; Rouzières, M.; Dechambenoit, P.; Mathonière, C.; Mathieu, F.; Dufour, I.; Ayela, C.; Clérac, R. Molecule-Based Microelectromechanical Sensors. 2017, arXiv:1701.01341. arXiv.org e-Print archive. https://arxiv.org/abs/1701.01341.
(46) Hernández, E. M.; Quintero, C. M.; Kraieva, O.; Thibault, C.; Bergaud, C.; Salmon, L.; Molnár, G.; Bousseksou, A. AFM Imaging of Molecular Spin-State Changes through Quantitative Thermomechanical Measurements. *Adv. Mater.* **2014**, *26*, 2889−2893.
(47) Urakawa, A.; Van Beek, W.; Monrabal-Capilla, M.; Galán-Mascarós, J. R.; Palin, L.; Milanesio, M. Combined, Modulation Enhanced X-ray Powder Diffraction and Raman Spectroscopic Study of Structural Transitions in the Spin Crossover Material [Fe(Htrz)$_2$(trz)](BF$_4$)†. *J. Phys. Chem. C* **2011**, *115*, 1323−1329.

DOI: 10.1021/acs.jpcc.8b10096
J. Phys. Chem. C 2019, 123, 6778−6786